Imaging Science in Dentistry 2015; 45: 67-72
http://dx.doi.org/10.5624/isd.2015.45.1.67

Arrested pneumatization of the sphenoid sinus mimicking intraosseous lesions of the skull base

Elnaz Jalali[1], Aditya Tadinada[1,*]

[1]*Department of Oral and Maxillofacial Radiology, University of Connecticut School of Dental Medicine, Farmington, CT, USA*

ABSTRACT

Arrested pneumatization of the sphenoid sinus is a developmental variant that is not always well recognized and is often confused with other pathologies associated with the skull base. This report describes the case of a patient referred for cone-beam computed tomography (CBCT) imaging for dental implant therapy. CBCT demonstrated a well-defined incidental lesion in the left sphenoid sinus with soft tissue-like density and sclerotic borders with internal curvilinear opacifications. The differential diagnoses included intraosseous lipoma, arrested pneumatization of the sphenoid sinus, chondrosarcoma, chondroid chordoma, and ossifying fibroma. The radiographic diagnosis of arrested pneumatization was based on the location of the lesion, its well-defined nature, the presence of internal opacifications, and lack of expansion. Gray-scale CBCT imaging of the area demonstrated values similar to fatty tissue. This case highlighted the fact that benign developmental variants associated with the skull base share similar radiographic features with more serious pathological entities. (***Imaging Sci Dent 2015; 45: 67-72***)

KEY WORDS: Pneumatization; Sphenoid Sinus; Cone-Beam Computed Tomography; Skull Base

The normal process of pneumatization of the skull base and paranasal sinuses starts in utero and develops through young adulthood.[1,2] It is known that the red bone marrow is replaced by the fatty marrow prior to the normal pneumatization process of the paranasal sinuses, including the sphenoid bones.[3,4] The process of marrow conversion occurs before epithelialization and the formation of the respiratory mucosa in the aerated sinus. In the sphenoid, the fatty conversion usually begins at around four months of age, and by 10-14 years of age, the fatty marrow is replaced by a fully pneumatized sinus lined by respiratory epithelium.[5,6] Any deviation from the normal developmental process presents as a developmental variation, including the absence, hypoplasia, or arrested pneumatization of the sinuses, with the latter resulting in the persistence of atypical fatty marrow adjacent to the sinus into adulthood.[7,8] Individuals with arrested pneumatization of the skull base are usually asymptomatic and the variant is most often discovered incidentally when imaging is performed for a separate cause. It is important to differentiate arrested pneumatization from more threatening conditions that may involve the central skull base in order to help the clinician choose the appropriate management approach. Some of the imaging features of this entity can closely mimic other benign fat-containing or ominous skull base lesions such as intraosseous lipoma, intraosseous hemangioma, hamartoma, fibrous dysplasia, and chordomas.[8-10]

Arrested pneumatization of the skull base is not well recognized among dentists and can often be confused with other pathologies associated with the skull base, which may lead to unnecessary invasive diagnostic procedures or interventions. As a result of greater appreciation of this entity by radiologists and higher resolution cone-beam computed tomography (CBCT), computed tomography (CT), and magnetic resonance image (MRI) scans, arrested pneumatization of the paranasal sinuses is now thought be significantly more common than previous estimates indicated and is thought to be underreported.

The aim of this study was to highlight the imaging fea-

Received September 8, 2014; Revised October 10, 2014; Accepted October 20, 2014
*Correspondence to: Dr. Aditya Tadinada
Department of Oral and Maxillofacial Radiology, University of Connecticut, School of Dental Medicine, 263 Farmington Ave., Farmington, CT 06030, USA
Tel) 1-869- 679- 2719, Fax) 1-860-679-4760, E-mail) tadinada@uchc.edu

tures of arrested pneumatization of the skull base to aid the clinician in recognizing this developmental variant. The presenting characteristics of arrested pneumatization of the skull base and a list of differential diagnoses for similar bony changes within the skull base are also described.

Case Report

A 47-year-old female patient was referred to the advanced oral and maxillofacial imaging center of the University of Connecticut School of Dental Medicine for a presurgical evaluation of implant sites in the maxilla using CBCT.

The CBCT scan was acquired with a Hitachi CBMercuRay CBCT unit (Hitachi Medical Corporation, Tokyo, Japan) with a nine-inch field of view at 120 kVp and 15 mA. During the radiographic interpretation of the acquired scan volume, an ellipsoid, well-demarcated, mixed-density lesion with multiple areas of mineralization was incidentally discovered in the greater sphenoid/basisphenoid area. The borders of this lesion were mildly hyperostotic. The lesion extended laterally from the midline to the right border of the greater sphenoid and sagittally to the basisphenoid, and did not communicate with the aerated portion of the remaining sphenoid sinus. A change in the normal pattern of bone trabeculae was noted inside the entity, along with multiple internal curvilinear calcifications. No mass effect was observed on the adjacent bony structures (Fig. 1). Given its location and non-aggressive radiographic appearance, the primary differential diagnoses were intraosseous lipoma, a benign fibro-osseous lesion, and arrested pneumatization.

Upon clinical examination, the patient did not show any neurological deficits or any other overt clinical symptoms. The patient's past medical history was unremarkable and no symptoms were reported of headache, deteriorating vision, or vertigo. The gray-scale CBCT values of the hypodense portion of the mass were measured. Using the gray-

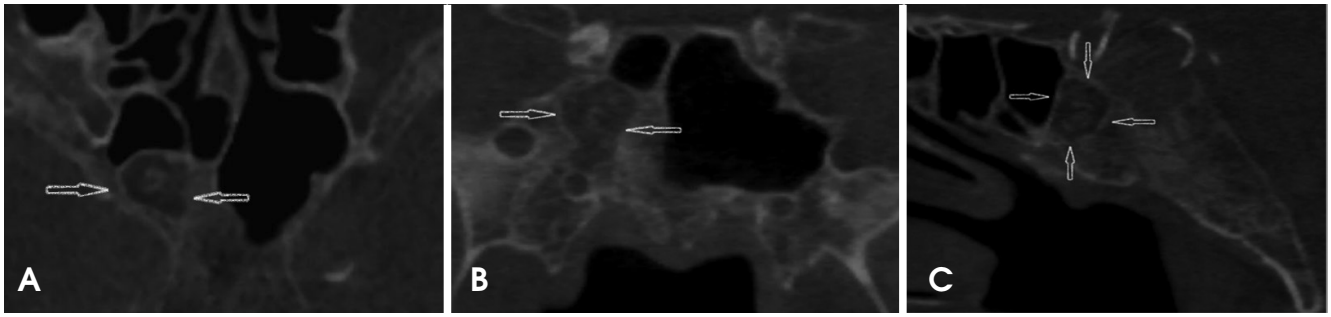

Fig. 1. The axial (A), coronal (B), and sagittal (C) images of a CBCT scan show the area of the arrested pneumatization of the right sphenoid sinus. The well-defined sclerotic borders, curvilinear internal calcifications, soft tissue density zones, and absence of any evidence of expansion or effect on the surrounding structures are visualized. The external morphology of the sphenoid bone appears to be normal.

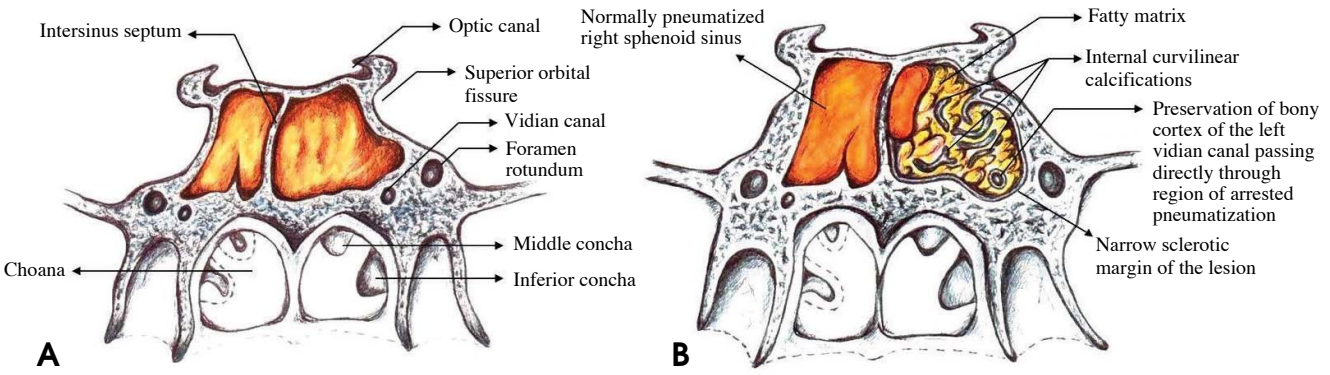

Fig. 2. A. A schematic diagram shows the normal pneumatization of the sphenoid sinus and the surrounding anatomic structures in this area. B. A schematic diagram shows arrested pneumatization of the left sphenoid sinus. The lesion has multiple foci of fat, narrow sclerotic margins, and internal curvilinear calcifications. The left vidian canal passes through the region of arrested pneumatization. Note the well-preserved bony cortex of the canal.

Table 1. Imaging features of intraosseous lesions of the skull base

Diagnosis	CT/CBCT	MRI-T1	MRI-T2 Fat Saturation	MRI-T1+Contrast
Arrested pneumatization	Non-expansile lesion with internal curvilinear calcification and foci of overt fat; sclerotic margin; variable degrees of loss to bone trabeculae; no cortical breach	Increased intensity	Decreased intensity	No enhancement
Intraosseous lipoma	Expansile lesion with internal fatty matrix and micro-calcifications; partial to complete loss of bony trabeculae; cortical breach is common	Increased or mixed signal intensity	Decreased or mixed signal intensity	No enhancement
Chordoma and chondrosarcoma	Expansile, destructive lesion with no fat contents; lobulated borders; may contain internal bone particulate matter/chondroid pattern of calcification with amorphous or stippled configuration; cortical breach is possible	Variable (the bulk of tumor is isointense or hypointense with localized areas of hyperintensity)	Increased or mixed signal intensity	Moderate to marked enhancement
Fibrous dysplasia and ossifying fibroma	Expansile, non-fat containing lesion; lobulated borders; sclerotic margins; internal foci of mineralization; the matrix may have an amorphous ground-glass appearance; cortical breach is possible	Variable (hypointense to intermediate signal intensity depending on the ratio of mineralized matrix to fibrous tissue)	Variable (hypointensity due to highly mineralized matrix; hyperintensity due to intralesional cystic components; mixed signal patterns due to mixed contents)	Variable
Intraosseus hemangioma	Expansile lesion; may or may not have fatty contents; mixed density lesion with a lacelike pattern of bone trabeculae; cortical breach is possible	Signal intensity may be increased (most commonly) or mixed	Increased intensity	Marked enhancement
Osteomyelitis and metastatic diseases	Expansile; multifocal areas of dense sclerosis, or lytic permeative/ erosive changes in the cortical or cancellous bone; cortical breach is possible	Decreased signal intensity	Increased signal intensity	Marked enhancement in the affected marrow space

CT: computed tomography, CBCT: cone beam computed tomography, MRI: magnetic resonance imaging

scale values of the dental CBCT, Hounsfield units were derived using the comprehensive method described in the studies performed by Mah et al.[11] and Reeves et al.[12] The corrected Hounsfield units in the CBCT acquisition were characteristic of fatty tissue, suggesting the presence of fat surrounding the central, scattered curvilinear calcifications. The margins of the lesion were sharp and sclerotic, suggesting non-aggressive growth. At this time, the following working radiographic differential diagnoses were considered: intraosseous lipoma, a fibro-osseous lesion, and arrested pneumatization. Since the patient was asymptomatic and the lesion lacked the classic characteristics of an aggressive entity or a malignancy, watchful observation was recommended. The patient had a follow-up CBCT scan 12 months after the placement of dental implants and no change in the size of the lesion was noted. Therefore, although the presence of adipose tissue was not confirmed histologically, the radiographic diagnosis of arrested pneumatization was established by the non-expansile nature of the lesion, its well-circumscribed sclerotic borders, the presence of internal curvilinear calcifications, the intact borders of the adjacent neural foramina, and, crucially, the location of the lesion at a normal pneumatization site.

Discussion

During normal development, a process known as red-to-yellow marrow conversion takes place, in which the adipose tissue within the red marrow increases in relative percentage. Several studies indicate that pneumatization of the cranial bones, such as the paranasal sinuses and mastoid air cells, only occurs after red-to-yellow conversion.[13] If the conversion process does not begin or is not completed, the pneumatization process is arrested and the area that is normally aerated is instead filled with yellow marrow. Arrested development is more associated with the sphe-

noid sinus and its known sites of accessory pneumatization, but cases involving the frontal and maxillary sinuses have also been reported.[3,14] While the reason for sphenoid predominance is not clear, the considerably greater variation in the extent of aeration in the sphenoid sinus compared to other paranasal sinuses may be related to the more frequent occurrence of arrested pneumatization at this site.[8] In the sphenoid bone, conversion from red to yellow marrow begins in the anterior portion (pre-sphenoid), moving posteriorly toward the clivus.[4,6,13] This process begins at about four months of age,[6] but significant conversion occurs by the age of two years.[4]

Several studies have presented different hypotheses to explain the relationship between aeration and bone marrow conversion of the sphenoid bone. Some authors have proposed that changes in the vasculature and temperature can act as promoters for sphenoid marrow conversion,[4,15] while others have postulated that the ratio of trabecular to cortical bone is the driving mechanism.[16] Despite this, relatively little is known about this process and why there may be a delay or failure to mature normally. Subsequently, the respiratory mucosa expands into areas of sphenoid fatty marrow conversion as the pneumatization process commences (Fig. 2A). When the conversion of fatty marrow adjacent to the sinus into the respiratory mucosa fails at some point in development, atypical fatty marrow persists into adulthood, which is why this phenomenon is described as arrested pneumatization. Patients with this benign developmental variant are most often asymptomatic and the entity is usually discovered incidentally.[3,4,7,8] On imaging, this process can be confused with more ominous skull base disease processes, especially if the radiologist is unaware of arrested pneumatization or its classic characteristics, resulting in unnecessary follow-up imaging, biopsy, or management.

Arrested pneumatization can be diagnosed when a lesion fulfills Welker's criteria:[8] (1) the lesion must be located at a site of normal pneumatization or a site of recognized accessory pneumatization; (2) the lesion should have sclerotic, well-circumscribed margins; (3) the lesion must be non-expansile; (4) the lesion should show fatty content; (5) on CT, internal curvilinear calcifications should be present; (6) any associated skull base foramina should retain a normal appearance.

The non-expansile nature of the lesion can best be evaluated at the inferior orbital fissure and vidian canal, which should not be displaced nor disrupted (Fig. 2B). The present case demonstrated all of the aforementioned features. Regarding the presence of adipose tissue, the gray-scale CBCT values of the hypodense portion of the mass were measured, and Hounsfield units were then derived using the comprehensive method described by Mah et al.[11] and Reeves et al.[12] The corrected Hounsfield units in the CBCT acquisition were characteristic of fatty tissue. Another approach to discern various tissue types on CBCT is to distinguish them based on density measurements acquired using pixel intensity values, which can then help distinguish benign lesions from possibly malignant lesions. The normal pixel intensity values for air in the sinuses are -700 to -1000 on the pixel intensity value scale. In this case, the area of the lesion measured approximately $+185$ to $+200$, which is considered higher than the normal values typically registered on the pixel intensity value scale for the sinuses. This pixel number range is typically associated with fatty tissue.

The formation of a pneumatized cavity in the sphenoid bone appears after a phase of bone marrow involution.[13] The signs of arrested pneumatization delineated by Welker[8] reflect the persistence of zones of bone marrow involution that failed to pneumatize. This process is different from hypoplasia of the sinus, in which the non-aerated segment of the sphenoid body displays a normal trabecular pattern. According to Kuntzler and Jankowski,[14] the signs of arrested pneumatization may possibly reflect the mode of formation of the paranasal sinuses.

Differentiating arrested pneumatization from more threatening lesions that might involve the skull base is important to obviate the need for additional interventions such as biopsy or surgery. The presence of local fat in these cases can be misleading for radiologists unfamiliar with this entity. The low-density and heterogeneous appearance on CT/CBCT might prompt concern for a lytic process. The high signal from fat on T1-weighted MRI might be suggestive of an infiltrative lesion such as a chordoma. However, in some rare cases there might be no evidence of fat content. Some central skull base lesions that share similar imaging features with arrested pneumatization are intraosseous lipoma, chordoma, chondrosarcoma, fibrous dysplasia, intraosseous hemangioma, ossifying fibroma, and metastases. Table 1 outlines typical imaging hallmarks that help differentiate arrested pneumatization from the aforementioned lesions.

Intraosseous lipoma, a variant of classical lipoma, is composed of mature adipocyte proliferation within the marrow of normal trabecular bone.[9] Although intraosseous lipoma can exhibit some overlapping characteristics with arrested pneumatization, such as internal mineralization, fat content, increased signal intensity on MRI-T1,

and decreased intensity on MRI-T2 fat saturation; these lesions are commonly expansile, a characteristic which allows them to differentiated from arrested pneumatization. In addition, intraosseous lipomas in the maxillofacial region arise in the maxilla and the mandible[17] more frequently than in the bones of the central skull base.

Chordomas and chondrosarcomas are other craniofacial lesions that should be differentiated from arrested pneumatization. Although chordomas more commonly develop in the vicinity of the sphenoid sinus, unlike arrested pneumatization, they are expansile and destructive and do not contain central regions containing fat.[18] Their MRI features[19] are presented in Table 1.

Instead of the fatty contents and curvilinear calcifications of arrested pneumatization, the internal matrix of fibrous dysplasia has an amorphous ground-glass appearance on CT imaging and contains no fat.[20]

Similar to arrested pneumatization, intraosseous hemangioma is generally asymptomatic unless it causes a mass effect on the surrounding structures. The CT and MRI features of hemangioma[21] are presented in Table 1.

Arrested pneumatization can be differentiated from ossifying fibroma through careful observation of the internal contents. While ossifying fibroma exhibits a ground-glass marrow pattern in CT images,[22] the internal pattern of arrested pneumatization is distinct and is characterized by curvilinear calcification and fatty contents.

Central skull base metastasis most commonly results from breast, lung, and prostate cancers, which account for 40%, 14%, and 12% of cases, respectively.[23] In CT images, metastatic disease can manifest as multifocal areas of dense sclerosis in the skull base, or may demonstrate lytic or permeative destruction of trabecular or cortical bone. Arrested pneumatization can be distinguished from skull base metastasis or osteomyelitis since it does not cause a permeative pattern of osseous destruction.[24] The relevant MRI features are presented in Table 1.

We reviewed the pertinent imaging features of arrested pneumatization that can simulate the imaging characteristics of well-known lesions that can from the central skull base, including metastatic disease, intraosseous lipoma, chordoma and chondrosarcoma, intraosseous hemangioma, and fibro-osseous lesions. This comprehensive approach more realistically reflects the imaging challenges that occur when assessing whether imaging findings in this region indicate a benign anatomical variant or ominous lesions. Recognition of this variation and its typical imaging features is important for radiologists in order to avoid unnecessary further workups, biopsy, or surgery, which could potentially result in an adverse outcome. If the area of arrested pneumatization does not satisfy all of the aforementioned diagnostic criteria, serial imaging and watchful observation can help assess whether a lesion is benign.

In conclusion, the imaging features of arrested pneumatization can often resemble those of other lesions in the central skull base, including metastatic disease, intraosseous lipoma, chordoma and chondrosarcoma, intraosseous hemangioma, and fibro-osseous lesions. When encountering a non-expansile lesion with internal soft or fatty tissue, curvilinear calcifications, and sclerotic well-defined margins at a site of normal pneumatization or of recognized accessory pneumatization, a differential diagnosis of arrested pneumatization must be considered.

References

1. Spaeth J, Krugelstein U, Schlondorff G. The paranasal sinuses in CT-imaging: development from birth to age 25. Int J Pediatr Otorhinolaryngol 1997; 39: 25-40.
2. Shah RK, Dhingra JK, Carter BL, Rebeiz EE. Paranasal sinus development: a radiographic study. Laryngoscope 2003; 113: 205-9.
3. Scuderi AJ, Harnsberger HR, Boyer RS. Pneumatization of the paranasal sinuses: normal features of importance to the accurate interpretation of CT scans and MR images. AJR Am J Roentgenol 1993; 160: 1101-4.
4. Aoki S, Dillon WP, Barkovich AJ, Norman D. Marrow conversion before pneumatization of the sphenoid sinus: assessment with MR imaging. Radiology 1989; 172: 373-5.
5. Jang YJ, KIM SC. Pneumatization of the sphenoid sinus in children evaluated by magnetic resonance imaging. Am J Rhinol 2000; 14: 181-5.
6. Szolar D, Preidler K, Ranner G, Braun H, Kern R, Wolf G, et al. Magnetic resonance assessment of age-related development of the sphenoid sinus. Br J Radiol 1994; 67: 431-5.
7. Degirmenci B, Haktanir A, Acar M, Albayrak R, Yücel A. Agenesis of sphenoid sinus: three cases. Surg Radiol Anat 2005; 27: 351-3.
8. Welker KM, DeLone DR, Lane JI, Gilbertson JR. Arrested pneumatization of the skull base: imaging characteristics. AJR Am J Roentgenol 2008; 190: 1691-6.
9. Srubiski A, Csillag A, Timperley D, Kalish L, Qiu MR, Harvey RJ. Radiological features of the intraosseous lipoma of the sphenoid. Otolaryngol Head Neck Surg 2011; 144: 617-22.
10. Politi M, Romeike BF, Papanagiotou P, Nabhan A, Struffert T, Feiden W, et al. Intraosseous hemangioma of the skull with dural tail sign: radiologic features with pathologic correlation. AJNR Am J Neuroradiol 2005; 26: 2049-52.
11. Mah P, Reeves TE, McDavid WD. Deriving Hounsfield units using grey levels in cone beam computed tomography. Dentomaxillofac Radiol 2010; 39: 323-35.
12. Reeves TE, Mah P, McDavid WD. Deriving Hounsfield units

using grey levels in cone beam CT: a clinical application. Dentomaxillofac Radiol 2012; 41: 500-8.
13. Taccone A, Oddone M, Occhi M, Dell'Acqua A, Ciccone MA. MRI "road-map" of normal age-related bone marrow. I. Cranial bone and spine. Pediatr Radiol 1995; 25: 588-95.
14. Kuntzler S, Jankowski R. Arrested pneumatization: witness of paranasal sinuses development? Eur Ann Otorhinolaryngol Head Neck Dis 2014; 131: 167-70.
15. Yonetsu K, Watanabe M, Nakamura T. Age-related expansion and reduction in aeration of the sphenoid sinus: volume assessment by helical CT scanning. AJNR Am J Neuroradiol 2000; 21: 179-82.
16. Gurevitch O, Slavin S, Feldman AG. Conversion of red bone marrow into yellow - Cause and mechanisms. Med Hypotheses 2007; 69: 531-6.
17. Burić N, Krasić D, Visnjić M, Katić V. Intraosseous mandibular lipoma: a case report and review of the literature. J Oral Maxillofac Surg 2001; 59: 1367-71.
18. Erdem E, Angtuaco EC, Van Hemert R, Park JS, Al-Mefty O. Comprehensive review of intracranial chordoma. Radiographics 2003; 23: 995-1009.
19. Neff B, Sataloff RT, Storey L, Hawkshaw M, Spiegel JR. Chondrosarcoma of the skull base. Laryngoscope 2002; 112: 134-9.
20. Daffner RH, Kirks DR, Gehweiler JA Jr, Heaston DK. Computed tomography of fibrous dysplasia. AJR Am J Roentgenol 1982; 139: 943-8.
21. Politi M, Romeike BF, Papanagiotou P, Nabhan A, Struffert T, Feiden W, et al. Intraosseous hemangioma of the skull with dural tail sign: radiologic features with pathologic correlation. AJNR Am J Neuroradiol 2005; 26: 2049-52.
22. Baumann I, Zimmermann R, Dammann F, Maassen MM. Ossifying fibroma of the ethmoid involving the orbit and the skull base. Otolaryngol Head Neck Surg 2005; 133: 158-9.
23. Greenberg HS, Deck MD, Vikram B, Chu FC, Posner JB. Metastasis to the base of the skull: clinical findings in 43 patients. Neurology 1981; 31: 530-7.
24. Kösling S, Neumann K, Brandt S. CT and MRI of intrinsic space-occupying lesions of the bony skull base. Radiologe 2009; 49: 598-607.